Original Article

Whole-cerebrum three-dimensional pseudo-continuous arterial spin labeling at 5T: reproducibility and preliminary application in moyamoya

Xiaoyuan Fan[1#], Zhonghui Li[1#], Guangsong Han[2#], Gan Sun[3], Hualu Han[4], Yuehui Hong[2], Shuo Chen[4], Hui You[1], Jun Ni[2], Guobin Li[4], Mingli Li[1], Feng Feng[1,5]

[1]Department of Radiology, Peking Union Medical College Hospital, Chinese Academy of Medical Sciences and Peking Union Medical College, Beijing, China; [2]Department of Neurology, Peking Union Medical College Hospital, Chinese Academy of Medical Sciences and Peking Union Medical College, Beijing, China; [3]Theranostics and Translational Research Center, National Infrastructures for Translational Medicine, Institute of Clinical Medicine, Chinese Academy of Medical Sciences and Peking Union Medical College, Beijing, China; [4]Shanghai United Imaging Healthcare, Shanghai, China; [5]State Key Laboratory of Complex Severe and Rare Diseases, Peking Union Medical College Hospital, Chinese Academy of Medical Sciences and Peking Union Medical College, Beijing, China

Contributions: (I) Conception and design: X Fan, Z Li, H Han, M Li; (II) Administrative support: S Chen, J Ni, G Li, M Li, F Feng; (III) Provision of study materials or patients: G Han, G Sun, Y Hong, S Chen; (IV) Collection and assembly of data: X Fan, Z Li, G Han; (V) Data analysis and interpretation: X Fan, Z Li, H Han, H You; (VI) Manuscript writing: All authors; (VII) Final approval of manuscript: All authors.

[#]These authors contributed equally to this work.

Correspondence to: Feng Feng, MD. Department of Radiology, Peking Union Medical College Hospital, Chinese Academy of Medical Sciences and Peking Union Medical College, No. 1 Shuaifuyuan, Dongcheng District, Beijing 100730, China; State Key Laboratory of Complex Severe and Rare Diseases, Peking Union Medical College Hospital, Chinese Academy of Medical Sciences and Peking Union Medical College, Beijing, China. Email: ffeng@pumch.cn; Mingli Li, MD. Department of Radiology, Peking Union Medical College Hospital, Chinese Academy of Medical Sciences and Peking Union Medical College, No. 1 Shuaifuyuan, Dongcheng District, Beijing 100730, China. Email: limingli@pumch.cn.

Background: Pseudo-continuous arterial spin labeling (PCASL) at 7T benefits from increased signal-to-noise ratio (SNR) and prolonged T1, but suffers from field inhomogeneities and increased specific absorption rate (SAR). We proposed that 5T magnetic resonance imaging (MRI) system may be a balanced choice for PCASL imaging. The aim of this study was to achieve whole-cerebrum PCASL imaging at ultra-high field 5T MRI system, assess the reproducibility and preliminarily explore its clinical application in moyamoya disease/syndrome.

Methods: Twenty healthy volunteers were prospectively recruited for the reproducibility analysis. Both single-delay and multi-delay PCASL sequences were scanned twice on the 5T MRI scanner separated by a 10-minute period. Uncorrected cerebral blood flow (uCBF) from single-delay arterial spin labeling (ASL), corrected cerebral blood flow (cCBF) and arterial transit time (ATT) from multi-delay ASL were computed. The reproducibility of uCBF, cCBF and ATT were evaluated by calculating intraclass correlation coefficient (ICC), within-subject coefficient of variation (wsCV) and Pearson correlation coefficients between twice scans in grey matter regions and white matter (WM). Also, 26 patients diagnosed with moyamoya disease/syndrome were included and underwent multi-delay PCASL. The severity of intracranial arteries was graded as magnetic resonance angiography (MRA) score using time-of-flight (TOF) MRA. The relationship between MRA score and cCBF/ATT were assessed by one-way analysis of variance and Pearson correlation analysis.

Results: uCBF, cCBF and ATT showed excellent reliability in all regions with ICCs ranging from 0.856 to 0.962, wsCVs ranging from 2.39% to 6.76% and Pearson correlation coefficients ranging from 0.865 to 0.966. Multi-delay ASL demonstrated superior reproducibility of CBF quantification compared to single-delay ASL in regions with heterogeneous transit time, including WM, occipital lobe, limbic system and subcortical

region. In patients with moyamoya disease/syndrome, those with higher anterior cerebral artery (ACA) or middle cerebral artery (MCA) scores exhibited lower cCBF (P<0.05). Correlation analysis showed that MRA score was negatively associated with cCBF (r=–0.540, P<0.001) and positively associated with ATT (r=0.515, P<0.001).

Conclusions: Whole-cerebrum PCASL imaging at 5T ultra-high field was achieved with good reproducibility and applied well in patients with moyamoya disease/syndrome, which offers a promising tool in the assessment of hemodynamic conditions in cerebrovascular diseases.

Keywords: Ultra-high field; 5T; arterial spin labeling (ASL); reproducibility; moyamoya disease

Submitted Oct 18, 2024. Accepted for publication Mar 14, 2025. Published online Apr 28, 2025.
doi: 10.21037/qims-24-2274
View this article at: https://dx.doi.org/10.21037/qims-24-2274

Introduction

Arterial spin labeling (ASL) magnetic resonance imaging (MRI) is a non-invasive technique that can acquire quantitative cerebral blood flow (CBF) by magnetically labeling water molecules in arterial blood as an endogenous tracer. The "ASL White Paper" has been accessible for nearly a decade, and a growing body of researches have confirmed the value of ASL technology in various central nervous system (CNS) diseases, such as brain tumors, cerebrovascular diseases and so on (1,2). However, the inherent limitations of ASL sequence, including low signal-to-noise ratio (SNR), restricted resolution and limited tracer half-life, still limit the clinical application of this technique (3).

As field strength increases, SNR is significantly elevated and blood T1 value gets prolonged. Nowadays, ASL at ultra-high field strengths, such as 7T, has been applied and expected to provide more accurate perfusion quantification. However, ASL MRI at 7T still meets two main challenges. One challenge is the field inhomogeneity that results in decreased labeling efficiency (4-7). Owing to reduced radiofrequency (RF) magnetic (B1+) field generated by the Tx elements below the brain at 7T, inversion efficiency of labeling RF pulses becomes insufficient and the perfusion signal diminishes consequently. The other challenge is the high specific absorption rate (SAR), which limits the use of high flip angle labeling pulse, background suppression pulse and spin-echo-type readout sequences, and ultimately leads to reduced spatial coverage. In the past few years, progress in ultra-high field ASL has been primarily focused on technical optimizations (8-10). Recently, an optimized pseudo-continuous arterial spin labeling (PCASL) sequence at 7T achieved whole-cerebrum imaging and kept SAR levels within the first level. Their study chose the Turbo-Fast Low Angle SHot (TFL) readout to reduce distortion and susceptibility artifacts, however, the longer readout duration still reduced SNR efficiency (11). Thus, it is not an easy work to apply ASL at 7T MRI system in clinical practice in a short term.

Recently, a 5T MRI system has been established, and a series of studies have confirmed its capability to produce superior quality images (12-14). Compared with previous MRI systems, 5T MRI system exhibits higher SNR than 3T. It also owns lower SAR, improved magnetic field homogeneity and comparable SNR compared with 7T; hence, it could be a balanced choice for SNR and inversion efficiency in PCASL imaging. Moreover, perfusion signal in white matter (WM) and subcortical area is not easy to detect for ASL with single post-labeling delay (PLD) time due to the poor sensitivity and heterogeneous transit time (15). Similarly, in patients with complex cerebrovascular diseases, single-delay ASL can also lead to inaccurate quantification because of arterial stenosis or collateral circulation. Confronted with these situations, 5T MRI can provide multi-delay PCASL with a super prolonged PLD (such as 3,500 ms), which helps measure the perfusion more accurately in regions with heterogeneous transit time and even cerebrovascular disease. However, the performance of 5T PCASL with either single PLD or multiple PLDs has not been reported yet.

The aim of this study was to achieve whole-cerebrum PCASL imaging at ultra-high field 5T MRI system, further assess the reproducibility of both single-delay and multi-delay ASL for the quantification of cerebral perfusion and preliminarily explore its clinical application in moyamoya disease/syndrome. We present this article in accordance with the STROBE reporting checklist (available at https://qims.amegroups.com/article/view/10.21037/qims-24-2274/rc).

Methods

The study was conducted in accordance with the Declaration of Helsinki and its subsequent amendments. This study was approved by the Medical Ethics Committee of the Peking Union Medical College Hospital (No. I-23PJ2044). Written consent was obtained from each subject.

Setup of PCASL imaging at 5T

The MR imaging was performed on a 5T MR scanner (uMR Jupiter, United Imaging Healthcare, China) with a 2Tx/48Rx head coil. In order to guarantee subject safety, SAR limits of head/trunk/extremities for the local transmit coil were set as 10/10/20 W/kg for long time (6 min) and 20/20/40 W/kg for short time (10 s), based on IEC International Standard 60601-2-33 (Table 201.104). Before ASL scan, third order shimming was conducted to reduce B0 inhomogeneity and B1 shimming to reduce B1+ inhomogeneity. A rough time-of-flight (TOF) vessel scout was scanned to localize the labeling plane, with the parameters detailed as: transverse, echo time (TE)/repetition time (TR) 3.1/18.1 ms, in-plane resolution 1.37×1.03 mm^2, thickness 1 mm, through-plane interpolation 2, field of view (FOV) 230×200×120 mm^3, compressed sensing factor 5, scan time 1 min 15 s. In order to achieve the whole-cerebrum cerebral perfusion measurement, the labeling plane was located below the brain parenchyma at the level of V3 segment of the vertebral arteries (VA) and perpendicular to both VA and internal carotid arteries (ICAs) for a robust quantitative measurement (3) (Figure S1A).

For the PCASL sequence, the acquisition used 3D gradient spin-echo (GRASE) readout for higher SNR and employed Partial Fourier and segmented readouts to reduce the acquisition windows for image sharpness. In the labeling module, RF pulse had a theoretically mean B1 of ~1.4 μT with each sub-pulse flip angle of 35°, pulse duration of 0.8 ms and pulse spacing of 0.7 ms. The PCASL labeling duration was set as 1,800 ms in this study for both single-delay and multi-delay PCASL. Besides, background suppression was conducted with a pre-saturation and 3 inversion pulses to suppress the static tissue signal for higher SNR. Vascular suppression pulse was used at multi-delay PCASL sequence to reduce intravascular signal. M0 scan was conducted before label/control acquisitions without labeling and background suppression modules.

Optimization and implementation of labeling parameters

To resolve the field inhomogeneity and achieve higher label efficiency, Bloch simulation and *in vivo* experiments were conducted to compare the inversion performances of labeling gradients, including average gradient (G_{avg}), maximum gradient (G_{max}) and their ratio ($G_{ratio} = G_{max}/G_{avg}$). Numerical simulation of flow-driven inversion was performed to evaluate the labeling efficiency at B1 inhomogeneity, B0 offset and pulsatile blood flow velocity (16). B1 scale represented the inhomogeneity ratio to the theoretical value, ranging from 20% to 120% with the step of 1%. Off-resonance phase shifted from 0 to 300 Hz with the step of 10 Hz. Blood flow velocity was chose from 0 to 80 cm/s with the step of 2 cm/s, covering the vast majority of both systolic velocity and diastolic velocity (17). T1 of blood was assumed to be 1,850 ms and T2 of arterial blood was 200 ms. Furthermore, three parameter sets (labeling 1: G_{avg} =1 & G_{ratio} =10; labeling 2: G_{avg} =0.6 & G_{ratio} =10; labeling 3: G_{avg} =0.3 & G_{ratio} =9) were chosen for following comparisons, where labeling 1 was recommended by the white paper (1), labeling 2 was commonly used at 3T and labeling 3 was assumed to have a certain tolerance to the field inhomogeneity especially at 5T. Other labeling parameters were listed in the previous section. The distributions of labeling efficiency with the function of flow velocity, B1 scale and B0 offset were simulated for three labeling sets (16). All simulations were performed within MATLAB 2022a (MathWorks, Natick, Massachusetts, USA). *In vivo* comparisons of labeling sets were characterized in 10 healthy volunteers (6 females, 36.9±13.3 years old) using an individual single-delay PCASL sequence. The optimal gradient setting was employed on the following experiments. In addition, B1 maps at the labeling plane were measured using a preconditioning RF pulse with TFL readout in another 8 volunteers (4 females, 50.7±10.8 years old) (18). Mean B1 scales at the locations of labeled arteries were measured by selecting 4 pixels separately at TOF vessel scout images and estimated the labeling efficiency based on the numerical simulation (Figure S1B,S1C).

Labeling efficiencies of different labeling gradients with regard to field inhomogeneities were shown in *Figure 1*. Comparing with labeling 1 and labeling 2, labeling 3 exhibited greater tolerance across the reduced B1+ and larger B0 offset frequency range, where mean velocity was assumed as 40 cm/s (*Figure 1A-1C*). Mean B1 scale in the labeling arteries across 8 volunteers was 64.7% with

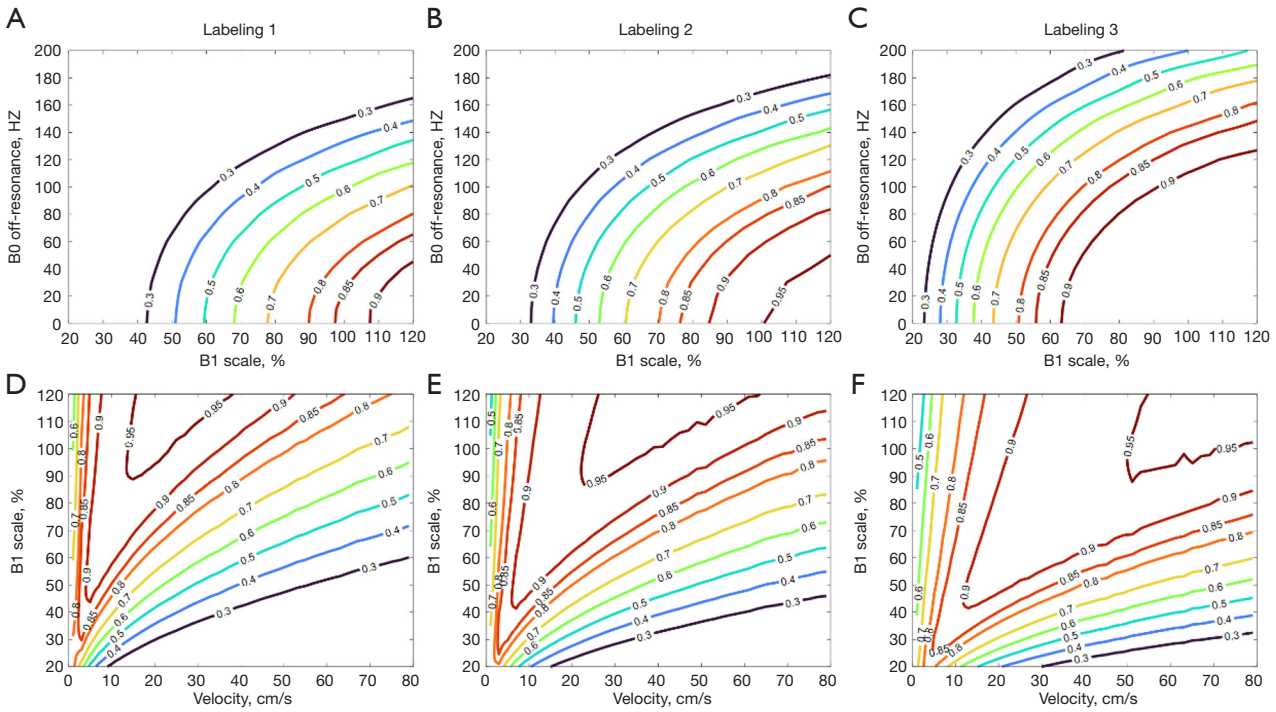

Figure 1 Simulated labeling efficiency maps. The upper row showed contour maps versus B1+ and B0 with the mean velocity as 40 cm/s for labeling 1 (A), labeling 2 (B), and labeling 3 (C). The lower showed contour maps versus velocity and B1+ with the resonance offset as 0 for labeling 1 (D), labeling 2 (E), and labeling 3 (F).

the range from 54.1% to 75.3%, indicating that labeling efficiency was achieved to be higher than 85% and increased to over 90% at average. Regarding to the flow velocity, labeling 3 showed a reduced labeling efficiency for low-velocity spins due to the substantial T2 decay during the gradual inversion (*Figure 1D-1F*). *In vivo* validations were conducted on single-delay PCASL sequences and mean perfusion signal was calculated for each labeling parameter set and shown in *Figure 2*. Quantitative evaluations revealed that traditional labeling parameter sets at 3T (labeling 1 and labeling 2) results in underestimation of perfusion due to the poor labeling efficiency.

The gray matter (GM) perfusion signal measured by labeling 3 (60.0±5.7 mL/100 g/min) was higher than labeling 1 (49.4±6.1 mL/100 g/min) and labeling 2 (55.7±7.0 mL/100 g/min). Overall, in order to provide a more robust labeling efficiency, the set of labeling 3 was used for further PCASL imaging.

Subjects

Twenty healthy adult volunteers were recruited between October 2023 and December 2023 for the reproducibility analysis. No participants had known or suspected cardiovascular diseases. No cerebrovascular diseases, neurodegenerative diseases, or other CNS disorders were observed on structural MRI. In addition, 30 patients diagnosed with moyamoya disease/syndrome were also scanned between December 2023 and April 2024 to preliminarily assess the clinical feasibility of the multi-delay ASL sequence. Patients who had poor image quality (n=1) and those with massive ischemic lesions that occupy ≥1 complete cortical region based on the Alberta Stroke Programme Early Computed Tomography Score on MRI (n=3) were excluded. Finally, 26 patients were included in the analysis.

Imaging protocol

Healthy volunteers were scanned with both single-delay and multi-delay PCASL sequences twice on the same 5T MRI scanner separated by a 10-minute rest period. Calibration was set to invalid between the within-session scans to delete all calibration results stored in the memory and re-run automatic pre-scanning. The uMR Jupiter monitored the

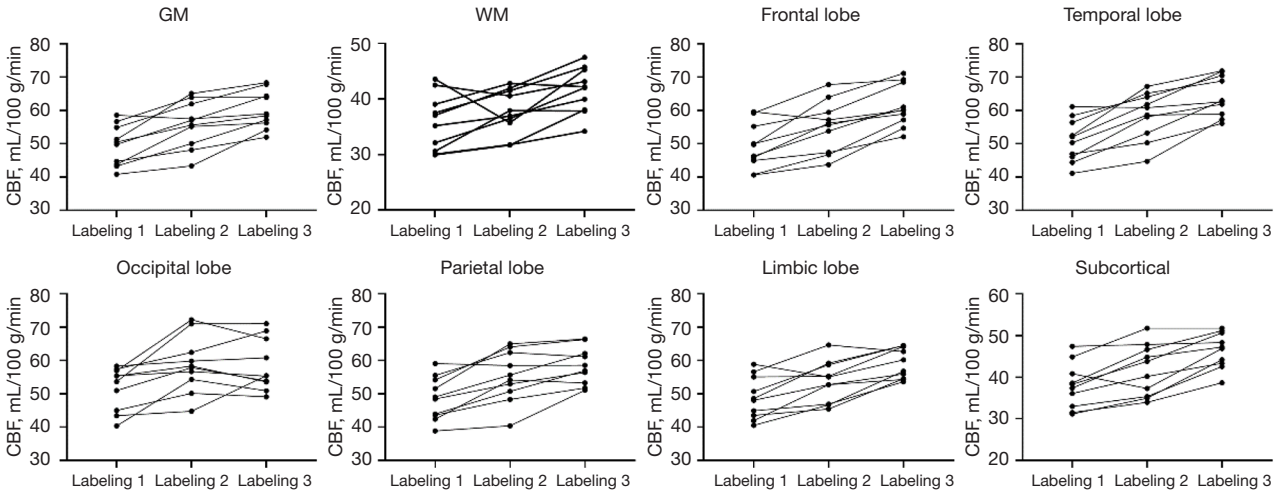

Figure 2 Quantitative comparisons of perfusion values of 3 labeling sets across brain lobes in 10 healthy subjects. CBF, cerebral blood flow; GM, gray matter; WM, white matter.

Table 1 Scanning parameters of single-delay and multi-delay ASL with single-shot gradient spin-echo readouts

Imaging parameter	Single-delay ASL	Multi-delay ASL
TR (ms)	6,485	6,089
TE (ms)	16.3	13.9
Labeling duration (ms)	1,800	1,800
Post-labeling delay (ms)	1,800	500, 1,000, 1,500, 2,000, 2,500, 3,000, 3,500
FOV (mm^3)	200×200×128	224×224×128
Voxel (mm^3)	2.5×2.5×4	3.5×3.5×4
Number of slices	32	32
Number of average	6	3/3/3/3/6/6/6
EPI factor	25	21
Turbo factor	27	27
Half Fourier along SPE	3/4	3/4
Acceleration factor along PE	3	3
Acquisition time (min:sec)	2:56	6:39

ASL, arterial spin labeling; EPI, echo planar imaging; FOV, field of view; PE, phase encoding; SPE, slice phase encoding; TE, echo time; TR, repetition time.

whole-body SAR and local SAR for subjects' safety. Patients were scanned with multi-delay PCASL and TOF magnetic resonance angiography (MRA) for clinical evaluation. For each subject, a rough TOF vessel scout was scanned firstly to localize the labeling plane of PCASL for a robust quantitative whole-cerebrum measurement (Figure S1) (3). Before the ASL scan, third order shimming was conducted to reduce B0 inhomogeneity and B1 shimming to reduce B1+ inhomogeneity.

The PCASL parameters are listed in *Table 1*. With the single-delay ASL sequence, a relatively higher spatial resolution of 2.5×2.5 mm^2 was set to reduce the partial volume effect. With the multi-delay ASL sequence, taking advantage of prolonged T1 and higher SNR, the longest PLD was set at 3,500 ms that longer than the conventional 2,500 ms at 3T, which was expected to achieve a more accurate depiction of cerebrovascular disorders. High-resolution anatomical images of T1 magnetization-prepared rapid acquisition gradient echo were also scanned for image registration, with parameters as below: sagittal, TE/TR 3.4/9.4 ms, inversion time (TI) 1,050 ms, resolution 0.7×0.7×0.7 mm^3, FOV 256×220×182 mm^3, flip angle 9°, artificial intelligence-assisted compressed sensing factor 3, scan time 4 min 7 s. TOF-MRA was used in moyamoya patients with scan parameters set as follows: transverse, TE/TR 3.8/19.5 ms, resolution 0.6×0.6×0.6 mm^3, FOV 200×230×96 mm^3, flip angle 15°, compressed sensing factor 4.5, scan time 5 min 51 s.

Image post-processing

Three quantitative perfusion parameters were analyzed on uOmnispace.MR (United Imaging Healthcare, China),

including uncorrected CBF (uCBF) from single-delay ASL, corrected CBF (cCBF) and arterial transit time (ATT) from multi-delay ASL. The general kinetic model fits the data for cCBF and ATT using non-linear least squares (19). In addition, motion-correction of the unsubtracted images was conducted using rigid-body transformations during post-processing. To scale subtracted ASL signals to the absolute CBF units, the M0 scan was used for calibration and here we set the T1 of blood as 1,850 ms (20), T1 of tissue as 1,500 ms (21), labeling efficiency as 72% and blood-brain partition coefficient as 0.9. Then, the absolute uCBF, cCBF and ATT maps were co-registered to 3D-T1 images on SPM12 (Wellcome Trust, England) and resliced to Montreal Neurological Institute space. Quantitative analyses focused on total GM, WM and subregions of GM using AAL3 template (22). In healthy volunteers, GM was segmented into different lobes, including frontal, parietal, temporal, occipital, limbic lobes and subcortical regions. Additionally, the GM was segmented based on perfusion territories, including the anterior cerebral artery (ACA), middle cerebral artery (MCA) and posterior cerebral artery (PCA) territories (23). In patients with moyamoya disease/syndrome, GM was segmented into different perfusion territories due to the disease affecting large arteries.

Imaging analysis in patients

The steno-occlusive severity of the main intracranial arteries was evaluated on MRA maximum-intensity projection images according to the Houkin's grading system (MRA score) (24). Specifically, the intracranial portion of ICA and the horizontal portion of MCA (M1) were scored as follows: 0 point, normal or minimum equivocal change of ICA/M1; 1 point, apparent stenosis of ICA/M1; 2 points, discontinuity of signal of ICA/M1; 3 points, invisible signal of ICA/M1. ACA and PCA were evaluated by assessing the visibility of the second segment of ACA (A2) and PCA (P2), as well as its distal branches. The scoring was conducted as follows: 0 point, normal signal intensity of A2/P2 and its distal; 1 point, signal decrease or loss of A2/P2 and its distal; 2 points, signal loss of ACA/PCA. Bilateral hemispheres were separately assessed, with the MRA score being the sum of ICA, MCA, ACA and PCA scores. Total MRA scores range from 0 to 10 points. Two radiologists (H.Y., 20 years of experience and Z.L., 8 years of experience in neuroradiology) evaluated the MRA score independently, blinded for the clinical and other imaging information. Disagreements were resolved by consensus.

Data analysis

Data analysis was conducted using SPSS Software V25.0 (IBM, Armonk, NY) and MedCalc Statistical Software V20.09 (MedCalc, Ostend, Belgium). Continuous variables were expressed as mean ± standard deviation (SD). In healthy volunteers, within-subject coefficient of variation (wsCV) and intra-class correlation coefficient (ICC) were calculated using MedCalc Statistical Software to assess the reproducibility of single-delay and multi-delay ASL, which aligns with the equations in previous studies (25,26). Specifically, the wsCV was computed by dividing the within-subject standard deviation by the mean of all measurements and multiplying by 100. A wsCV value close to 0 indicates high reproducibility. For the ICC calculation, the two-way random model with absolute agreement was chosen because of the aim that the results from two scans were not only highly correlated but also consistent in terms of absolute values. And the 'single measures' results were selected as ICC values. ICC values range between 0 and 1, and the reliability was interpreted as poor (<0.40), fair (0.41–0.59), moderate (0.60–0.74) and excellent (≥0.75). Correlation coefficient plots and Bland-Altman plots were generated to evaluate the measurement agreements between the two repeated scans. A paired *t*-test was used to compare CBF values obtained from the first and second scans. One-way analysis of variance was used to compare the cCBF among patients with different ACA and MCA scores. Bonferroni correction was performed for multiple comparisons. The correlation between MRA score and cCBF/ATT was evaluated by Pearson correlation analysis. $P<0.05$ was considered statistically significant.

Results

Reproducibility analysis of single-delay and multi-delay ASL

All 20 healthy volunteers successfully completed the protocol (10 males, 35.5±14.9 years old). No significant difference was found in uCBF, ATT and cCBF values between the two scans (all $P>0.05$). In the Bland-Altman analysis, the plots were randomly distributed without dependency within 90% confidence intervals (Figure S2).

Reproducibility analysis of uCBF by single-delay PCASL is reported in *Table 2*. The reproducibility analysis showed high ICCs and consistent wsCVs in GM (ICC =0.938, wsCV =3.81%), WM (ICC =0.873, wsCV =3.64%) and all other anatomical and vascular segments (ICCs >0.85 and

Table 2 Reproducibility analysis of uCBF from single-delay ASL

Region	Scan (mL/100 g/min)	Rescan (mL/100 g/min)	ΔuCBF† (mL/100 g/min)	ICC	wsCV (%)
GM	55.62±8.29	56.10±8.78	2.35±1.94	0.938	3.81
WM	39.15±4.03	39.61±4.04	1.54±1.36	0.873	3.64
Frontal	57.23±8.27	57.68±8.25	2.42±2.09	0.926	3.90
Parietal	54.17±8.91	54.47±9.28	2.26±1.86	0.949	3.76
Temporal	59.57±9.40	60.11±9.93	2.41±1.99	0.949	3.66
Occipital	53.42±9.27	53.91±10.63	3.68±3.66	0.867	6.76
Limbic	53.86±7.39	54.59±7.45	2.66±2.28	0.891	4.52
Subcortical	42.46±5.95	42.95±5.72	2.08 ±1.52	0.904	4.22
ACA	60.54±8.60	60.70±8.46	2.75±1.90	0.924	3.87
MCA	60.15±9.38	60.77±9.77	2.27±2.13	0.948	3.60
PCA	51.00±8.66	51.07±9.06	2.69±2.16	0.926	4.73

Data are presented as mean ± standard deviation. †, the absolute difference between scan and rescan. ACA, anterior cerebral artery; ASL, arterial spin labeling; GM, gray matter; ICC, intraclass correlation coefficient; MCA, middle cerebral artery; PCA, posterior cerebral artery; uCBF, uncorrected cerebral blood flow; WM, white matter; wsCV, within-subject coefficient of variation.

wsCVs <7%). For anatomical partitions, uCBF in parietal and temporal lobes reached the highest ICC (0.949) and that in WM reached the lowest wsCV (3.64%). In terms of vascular territories, uCBF in MCA reached the highest ICC (0.948) and the lowest wsCV (3.60%). Correlation analysis of the test-retest measurements of uCBF are shown in *Figure 3A,3B*. The Pearson correlation coefficients of uCBF were higher than 0.85 in GM, WM and all ROIs. Among them, the Pearson correlation coefficients for the parietal (0.948), temporal lobes (0.949) and MCA (0.949) were the highest.

Reproducibility analysis of ATT and cCBF by multi-delay PCASL are reported in *Table 3*. Both ATT and cCBF showed excellent reproducibility in GM, WM and all regions with ICCs higher than 0.85 and wsCVs lower than 7%. The reproducibility of ATT was similar in GM (ICC =0.951 and wsCV =2.84%) and WM (ICC =0.956 and wsCV =2.39%). Likewise, the reproducibility of cCBF was similar in GM (ICC =0.948, wsCV =4.58%) and WM (ICC =0.949, wsCV =4.38%). Among the different ROIs, the cCBF in the subcortical region reached the highest ICC (0.955) and the lowest wsCV (3.78%). Correlation analysis of the test-retest measurements of ATT and cCBF are shown in *Figure 3C-3F*. In GM, WM and all ROIs, the correlation analysis showed strong test-retest agreements with Pearson correlation coefficients higher than 0.85 (all P<0.001). WM and subcortical cCBF showed the highest correlation coefficients among all of the anatomic ROIs (r=0.956 and 0.955, respectively).

While both uCBF and cCBF exhibited good reproducibility, the ICCs of uCBF were relatively lower in WM, occipital, limbic and subcortical regions compared to other regions. Moreover, the ICCs of cCBF showed improvement in these same areas compared to uCBF. Also in the aforementioned areas, the correlation coefficients of cCBF were further increased compared with uCBF, especially in WM and subcortical region. A representative case of the test-retest analysis is shown in *Figure 4*.

Multi-delay ASL in moyamoya disease/syndrome

A total of 26 patients (11 males, 40.9±11.9 years old) with moyamoya disease or syndrome were analyzed. cCBF in the MCA territory with a score of 3 points (35.47±9.30 mL/100 g/min) was significantly lower than that with scores of 0 point (57.03±9.34 mL/100 g/min, P<0.001), 1 point (51.17±9.14 mL/100 g/min, P=0.001) and 2 points (47.38±8.97 mL/100 g/min, P=0.014). Also, MCA territories with a score of 2 points had lower CBF than those with 0 point (P=0.043, *Figure 5A*). cCBF in the ACA territory with a score of 2 points (37.90±10.20 mL/100 g/min) was significantly lower than that with a score of 0 point (57.11±10.87 mL/100 g/min, P<0.001, *Figure 5B*). Correlation analyses showed the MRA score was negatively

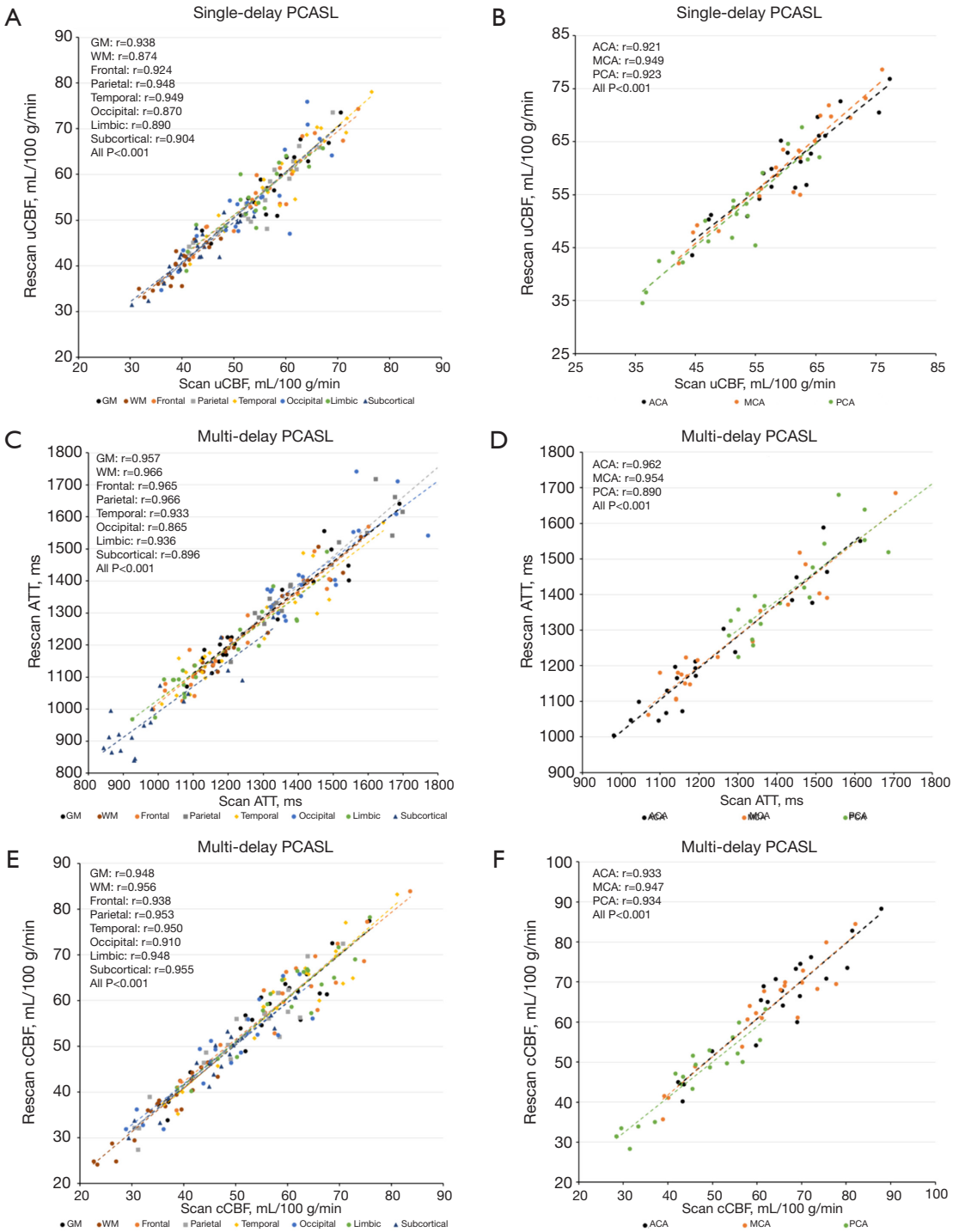

Figure 3 Correlation analysis of the test-retest measurements of uCBF, ATT and cCBF. (A) The test-retest measurements of uCBF in GM, WM and different lobes; (B) the test-retest measurements of uCBF within perfusion territories; (C) the test-retest measurements of ATT in GM, WM and different lobes; (D) the test-retest measurements of ATT within perfusion territories; (E) the test-retest measurements of cCBF in GM, WM and different lobes; (F) the test-retest measurements of cCBF within perfusion territories. ACA, anterior cerebral artery; ATT, arterial transit time; cCBF, corrected cerebral blood flow; GM, gray matter; MCA, middle cerebral artery; PCA, posterior cerebral artery; PCASL, pseudo-continuous arterial spin labeling; uCBF, uncorrected cerebral blood flow; WM, white matter.

Table 3 Reproducibility analysis of ATT and cCBF

Region	ATT					cCBF				
	Scan (ms)	Rescan (ms)	ΔATT† (ms)	ICC	wsCV (%)	Scan (mL/100 g/min)	Rescan (mL/100 g/min)	ΔcCBF† (mL/100 g/min)	ICC	wsCV (%)
GM	1,299.08±137.80	1,284.66±158.45	39.55±34.43	0.951	2.84	55.58±11.25	56.32±11.27	3.16±1.83	0.948	4.58
WM	1,278.91±150.56	1,260.53±136.21	32.40±28.88	0.956	2.39	35.75±7.02	36.73±6.98	2.08±0.87	0.949	4.38
Frontal	1,222.83±185.05	1,214.10±168.28	39.32±30.10	0.962	2.85	60.11±11.96	60.81±11.81	3.55±2.22	0.939	4.86
Parietal	1,452.57±178.87	1,432.26±171.55	36.43±34.29	0.960	2.42	50.43±11.78	51.45±11.92	3.16±1.95	0.952	5.11
Temporal	1,235.73±179.99	1,220.78±159.00	49.43±43.86	0.926	3.76	59.62±12.14	60.02±12.61	3.14±2.29	0.951	4.55
Occipital	1,486.13±167.53	1,458.32±156.19	65.24±59.28	0.856	4.19	47.75±10.19	48.68±9.98	3.70±2.23	0.910	6.29
Limbic	1,161.62±156.78	1,159.39±135.74	43.84±34.02	0.929	3.35	58.79±10.88	59.41±10.89	3.10±1.58	0.949	4.15
Subcortical	1,008.59±144.39	997.93±128.13	49.25±41.09	0.892	4.37	45.98±8.34	46.55±8.07	2.05±1.42	0.955	3.78
ACA	1,249.55±190.06	1,237.73±176.40	43.97±28.66	0.960	2.96	64.68±12.54	65.22±12.67	3.94±2.27	0.936	4.92
MCA	1,283.54±178.06	1,270.92±161.77	41.10±36.23	0.949	3.00	61.79±12.67	62.48±12.72	3.48±2.23	0.948	4.67
PCA	1,445.64±151.05	1,420.10±139.51	57.24±44.85	0.878	3.55	46.15±10.24	46.61±9.74	3.20±1.70	0.935	5.50

Data are presented as mean ± standard deviation. †, the absolute difference between scan and rescan. ACA, anterior cerebral artery; ATT, arterial transit time; cCBF, corrected cerebral blood flow; GM, gray matter; ICC, intraclass correlation coefficient; MCA, middle cerebral artery; PCA, posterior cerebral artery; WM, white matter; wsCV, within-subject coefficient of variation.

associated with cCBF (r=–0.540, P<0.001, *Figure 5C*) and positively associated with ATT (r=0.515, P<0.001, *Figure 5D*). Representative cases are shown in *Figure 6*.

Discussion

In this study, we achieved whole-cerebrum PCASL imaging based on GRASE at an ultra-high field 5T with high resolution and clinically acceptable scan time. This approach showed excellent test-retest reproducibility for measuring cerebral perfusion by both single-delay ASL and multi-delay ASL. And multi-delay ASL further improved the stability and accuracy of CBF quantification compared to single-delay ASL in regions with heterogeneous transit time, such as the WM and subcortical region. Our findings also validated its clinical feasibility in a cohort of patients with moyamoya disease/syndrome.

The PCASL imaging at 5T with high resolution and whole-cerebrum coverage was optimized by combining 3D GRASE readout, third-order B0 shimming and optimal gradient. PCASL is recommended for its better SNR and reproducibility compared to pulsed ASL (PASL) (1). However, previous studies often used PASL instead of PCASL at 7T to overcome the SAR constraint imposed by PCASL labeling pulses (9,27). Shorter labeling duration, increased labeling interval, smaller-than-optimal flip angle or VERSE pulse would be helpful to achieve PCASL imaging but sacrifice the labeling efficiency (28). Here on the 5T system, the SAR value of same sequence is less than that on 7T due to the positive relationship between SAR and B0 (29), which allows a commonly-used labeling pulse train to achieve high labeling efficiency and apply PCASL. We monitored the whole-body SAR and local SAR for subjects' safety during 5T scanning, and none of the SAR values exceeded the SAR limits based on IEC International Standard 60601-2-33 (Table 201.104). Moreover, several studies tried to resolve the B0 offset at 7T using high-order shimming or "prescan" calibration (30,31). We found that a third-order B0 shimming could achieve relatively small off-resonance in preliminary experiments. Besides, for B1 inhomogeneity at ultra-high field, reduced B1 below the brain in particular degrades the labeling efficiency. Most previous studies at 7T attempted to raise the location of the labeling slab but limited the imaging coverage (6,9,32). It is worth noting that we achieved high labeling efficiency and SNR at 5T by optimizing the labeling parameters of average gradient and maximum gradient based on the field distribution without sacrificing the image coverage (32).

Recently, Zhao *et al.* firstly achieved PCASL at 7T with whole-cerebrum coverage by combining a new set of labeling parameters, OPTIM BS pulse, and accelerated 3D TFL readout (11). Their research showed TFL-PCASL

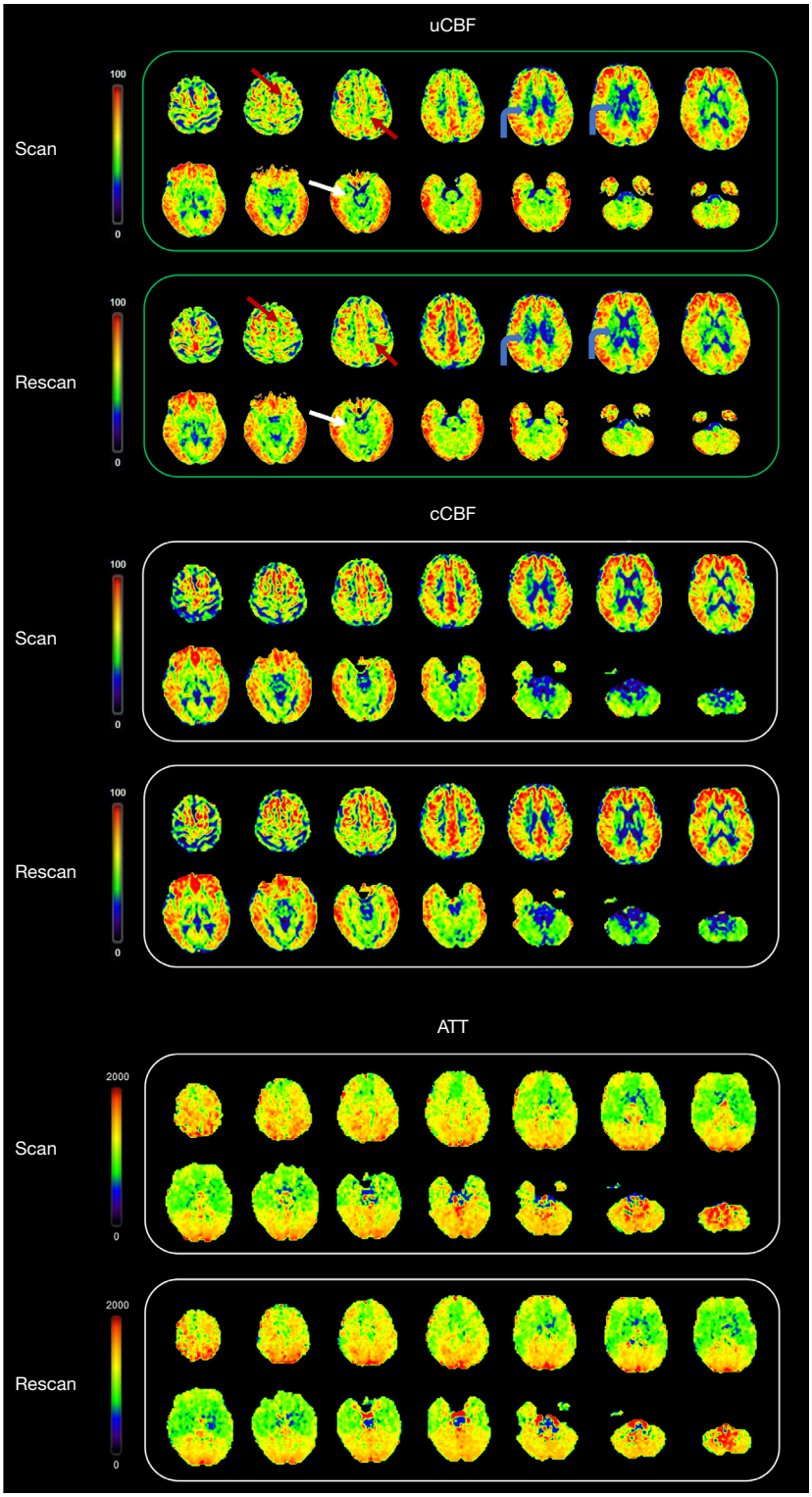

Figure 4 A representative case of the test-retest analysis of ATT, cCBF and uCBF. On uCBF maps generated by single-delay ASL, minor perfusion differences are noted between two scans within the white matter (red arrows), subcortical region (curve arrows) and limbic system (white arrow). On cCBF and ATT maps generated by multi-delay ASL, perfusion in these regions is more stable. ATT, arterial transit time; ASL, arterial spin labeling; cCBF, corrected cerebral blood flow; uCBF, uncorrected cerebral blood flow.

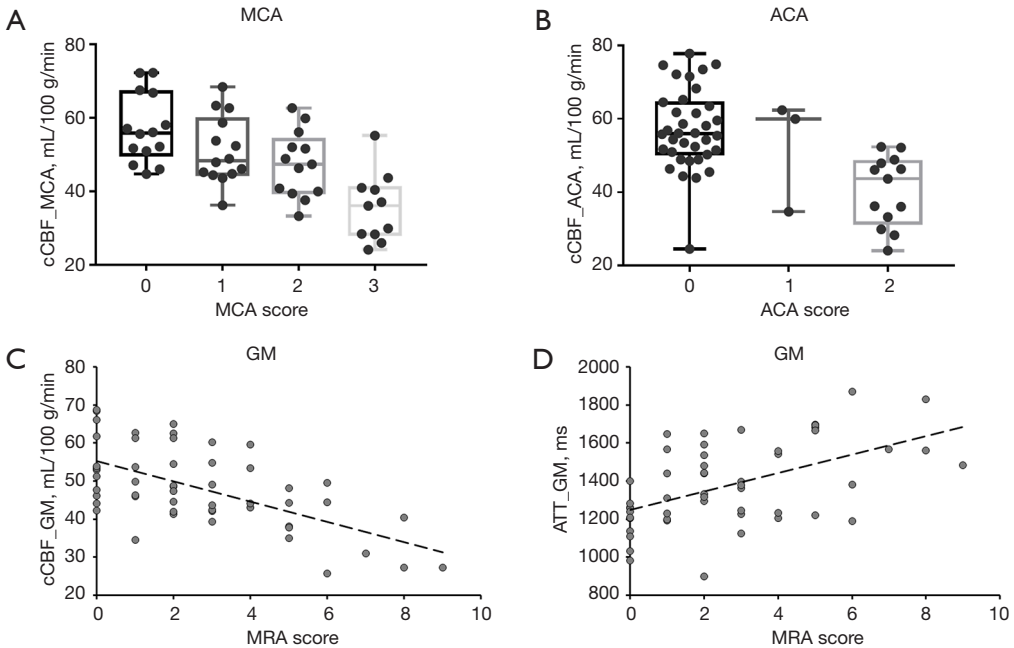

Figure 5 Relationship between cCBF, ATT and MRA score. (A) Comparison of cCBF in MCA territory among groups with different MCA scores; (B) comparison of cCBF in ACA territory among groups with different ACA scores; (C) comparison of cCBF in GM among groups with different MRA scores; (D) comparison of ATT in GM among groups with different MRA scores. ACA, anterior cerebral artery; ATT, arterial transit time; cCBF, corrected cerebral blood flow; GM, gray matter; MCA, middle cerebral artery; MRA, magnetic resonance angiography.

had a better reproducibility of CBF than GRASE-PCASL at 7T, but this improvement compromised on SNR and image sharpness. The GRASE-PCASL at 5T showed higher ICCs and similar wsCVs of CBF compared with 7T TFL-PCASL, which indicated that the 5T system may be a reliable alternative for high-resolution ASL.

The reproducibility of PCASL has been explored a lot at 3T and presents with good performance. Generally, in 3T ASL test-retest studies where two scans were conducted within the same session, wsCV values were typically between 5% and 10% (23,33-36). In the current study, the values of wsCV for both single-delay and multi-delay ASL were mostly within 5% and not higher than 7% in all regions, indicating a superior within-subject stability of 5T ASL (23). The ICCs of CBF varied from 0.86 to 0.95 steadily, which was similar with 3T ASL studies (23,33,34,36). The previous study by Mezue *et al.* showed fair to excellent reproducibility of ATT on 3T (wsCVs =1.35–4.54%, ICCs =0.53–0.91) for short intervals (36). Our wsCV values matched this range, but the ICC values were further improved. It may be more reliable to compare ATT differences among subjects, such as patients *vs.* controls by using 5T multi-delay ASL instead of 3T. Moreover, this study showed ATT exhibited even lower wsCV values compared to cCBF in all regions. The excellent repeatability not only means ATT itself as a reliable parameter of hemodynamics, but allows for more reliable measurement of cCBF (26).

Although both single-delay ASL and multi-delay ASL showed excellent reproducibility, our findings emphasized that cCBF had better reproducibility than uCBF in regions with heterogeneous transit time, especially in the WM and subcortical region. The ICCs of cCBF in the WM and subcortical region were higher compared with those reported in prior studies conducted on 3T scanners using both single-delay and multi-delay PCASL (33,34), and similar to the ICC values obtained with long-label PCASL (23). The perfusion signal is relatively low in WM and heterogeneous in the subcortical region; hence, these regions are sensitive to errors or GM-WM contamination (37). Higher SNR and resolution at 5T reduce the influence of co-registration errors or partial volume effects. More importantly, multi-delay ASL achieves CBF quantification corrected by ATT and we conducted a quite long PLD of 3,500 ms, which enables more labeled water protons flow into brain tissue to

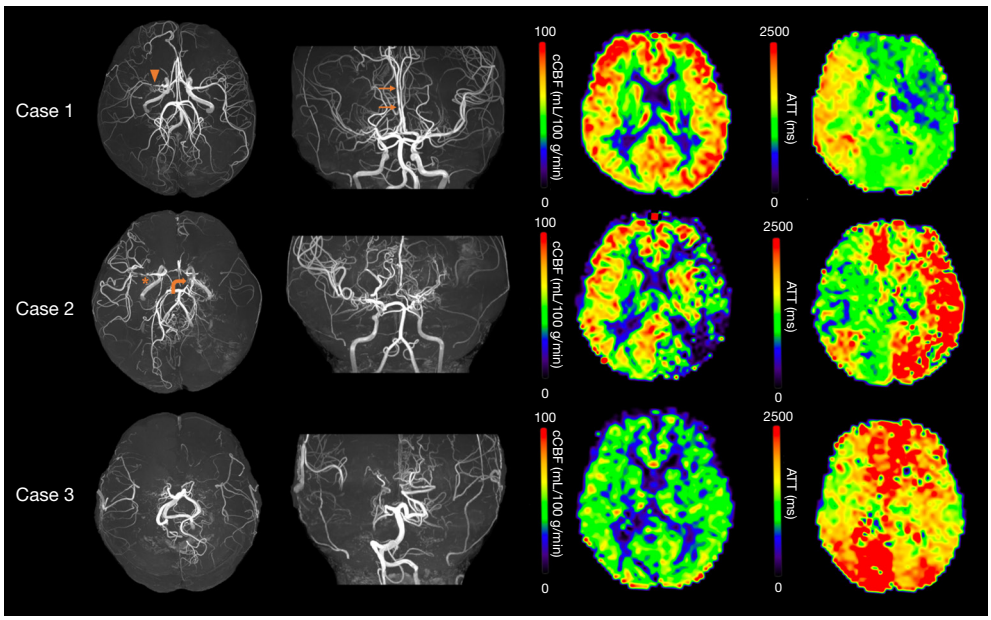

Figure 6 Representative cases of patients with moyamoya disease/syndrome. Case 1. A 26-year-old female patient with moyamoya syndrome. MRA images reveal signal discontinuity of M1 (MCA score =2, arrowhead) and signal decrease of A2 (ACA score =1, arrow). On cCBF and ATT maps, slightly reduced cCBF and prolonged ATT are observed within the territory of the right MCA territory, in contrast to the left MCA territory. Case 2. A 28-year-old male patient with moyamoya syndrome. In the right hemisphere, MRA images reveal apparent stenosis of M1 (MCA score =1, asterisk), signal loss of ACA (ACA score =2). In the left hemisphere, ICA stenosis is observed (curved arrow, ICA score =1), accompanied by signal loss of MCA (MCA score =3) and signal decrease of PCA (PCA score =1). Correspondingly, significantly reduced cCBF and prolonged ATT are observed within the territories of the left MCA and PCA territory, as depicted on the cCBF and ATT maps. Case 3. A 64-year-old female patient with bilateral moyamoya disease. MRA images show no depiction of ICA, MCA and ACA (ICA score =3, MCA score =3, ACA score =2), a diminished signal in right PCA (PCA score =1). This patient exhibited significantly prolonged ATT and decreased cCBF values compared to the previous two patients. ACA, anterior cerebral artery; ATT, arterial transit time; cCBF, corrected cerebral blood flow; ICA, internal carotid artery; MCA, middle cerebral artery; MRA, magnetic resonance angiography; PCA, posterior cerebral artery.

reflect the real level of brain perfusion (38).

Moyamoya disease/syndrome is characterized by progressive stenosis or occlusion of the distal ICA, ACA and MCA. Assessment of cerebral hemodynamics through various imaging techniques is essential for treatment decision and therapeutic efficacy evaluation (39). The MRA score represents the severity of intracranial arterial steno-occlusions and is significantly consistent with Suzuki's angiographic stages (24). Previous studies have demonstrated that PCASL can effectively identify hemodynamic impairment at different stages of moyamoya disease (40,41). Our results are consistent with their results. Since the reproducibility of multi-delay ASL was improved at 5T, it may be a potential tool for more stable and accurate assessments of moyamoya disease/syndrome and other cerebrovascular diseases with prolonged ATT.

Limitations

There are several limitations in this study. First, this study only evaluated the reproducibility of 5T ASL with a short interval of 10 minutes and without varying subject position, which mainly reflected the measurement errors. Longitudinal reproducibility with intervals over days or months are also important to reflect the influence of physiological factors on 5T ASL. Second, vital sign data such as blood pressure or arterial oxygen saturation were not collected from subjects; thus, the exact contributions of physiologic fluctuations to the variation of ASL were unclear. Third, this study did not perform ASL at 7T scanner. Differences in vendors, hardware equipment such as coil system and blood T1 values make it difficult to maintain consistent imaging protocols across 5T and 7T

MRI systems.

Conclusions

In conclusion, we presented whole-cerebrum PCASL imaging at ultra-high field 5T MRI system with good reproducibility. CBF can be reliably measured by multi-delay ASL even in regions with a heterogeneous transit time, especially in the WM and subcortical region. 5T MRI offers a promising tool for the efficient and accurate assessment of cerebrovascular diseases.

Acknowledgments

None.

Footnote

Reporting Checklist: The authors have completed the STROBE reporting checklist. Available at https://qims.amegroups.com/article/view/10.21037/qims-24-2274/rc

Funding: This work was supported by the National Nature Science Foundation of China Grants (Nos. 82071899 and 82371946), the National Postdoctoral Researcher Funding Program (No. GZC20240138), the Beijing Natural Science Foundation Grant (No. 7222131), and the National High Level Hospital Clinical Research Funding (No. 2022-PUMCH-B-067).

Conflicts of Interest: All authors have completed the ICMJE uniform disclosure form (available at https://qims.amegroups.com/article/view/10.21037/qims-24-2274/coif). H.H., S.C., and G.L. are employees of United Imaging Healthcare. The other authors have no conflicts of interest to declare.

Ethical Statement: The authors are accountable for all aspects of the work in ensuring that questions related to the accuracy or integrity of any part of the work are appropriately investigated and resolved. The study was conducted in accordance with the Declaration of Helsinki and its subsequent amendments. This study was approved by the Medical Ethics Committee of the Peking Union Medical College Hospital (No. I-23PJ2044) and informed consent was taken from all the patients.

References

1. Alsop DC, Detre JA, Golay X, Günther M, Hendrikse J, Hernandez-Garcia L, Lu H, MacIntosh BJ, Parkes LM, Smits M, van Osch MJ, Wang DJ, Wong EC, Zaharchuk G. Recommended implementation of arterial spin-labeled perfusion MRI for clinical applications: A consensus of the ISMRM perfusion study group and the European consortium for ASL in dementia. Magn Reson Med 2015;73:102-16.
2. Xiao Y, Chen S, Zhang Z, Huang J, Gui Y, Luo D, Deng X, Dai J, Xiao X. Three-dimensional pseudocontinuous arterial spin labeling with dual postlabeling delay for reflecting cerebral blood flow regulation in patients with hydrocephalus: a retrospective cross-sectional study. Quant Imaging Med Surg 2024;14:5861-76.
3. Lindner T, Bolar DS, Achten E, Barkhof F, Bastos-Leite AJ, Detre JA, et al. Current state and guidance on arterial spin labeling perfusion MRI in clinical neuroimaging. Magn Reson Med 2023;89:2024-47.
4. Hernandez-Garcia L, Aramendía-Vidaurreta V, Bolar DS, Dai W, Fernández-Seara MA, Guo J, et al. Recent Technical Developments in ASL: A Review of the State of the Art. Magn Reson Med 2022;88:2021-42.
5. Dury RJ, Falah Y, Gowland PA, Evangelou N, Bright MG, Francis ST. Ultra-high-field arterial spin labelling MRI for non-contrast assessment of cortical lesion perfusion in multiple sclerosis. Eur Radiol 2019;29:2027-33.
6. Ghariq E, Teeuwisse WM, Webb AG, van Osch MJ. Feasibility of pseudocontinuous arterial spin labeling at 7 T with whole-brain coverage. MAGMA 2012;25:83-93.
7. Teeuwisse WM, Webb AG, van Osch MJP. Arterial spin labeling at ultra-high field: All that glitters is not gold. International Journal of Imaging Systems and Technology 2010;20:62-70.
8. Wang Y, Moeller S, Li X, Vu AT, Krasileva K, Ugurbil K, Yacoub E, Wang DJ. Simultaneous multi-slice Turbo-FLASH imaging with CAIPIRINHA for whole brain distortion-free pseudo-continuous arterial spin labeling at

3 and 7 T. Neuroimage 2015;113:279-88.
9. Zimmer F, O'Brien K, Bollmann S, Pfeuffer J, Heberlein K, Barth M. Pulsed arterial spin labelling at ultra-high field with a B 1 (+) -optimised adiabatic labelling pulse. MAGMA 2016;29:463-73.
10. Saïb G, Koretsky AP, Talagala SL. Optimization of pseudo-continuous arterial spin labeling using off-resonance compensation strategies at 7T. Magn Reson Med 2022;87:1720-30.
11. Zhao C, Shao X, Shou Q, Ma SJ, Gokyar S, Graf C, Stollberger R, Wang DJ. Whole-Cerebrum distortion-free three-dimensional pseudo-continuous arterial spin labeling at 7T. Neuroimage 2023;277:120251.
12. Wei Z, Chen Q, Han S, Zhang S, Zhang N, Zhang L, Wang H, He Q, Cao P, Zhang X, Liang D, Liu X, Li Y, Zheng H. 5T magnetic resonance imaging: radio frequency hardware and initial brain imaging. Quant Imaging Med Surg 2023;13:3222-40.
13. Shi Z, Zhao X, Zhu S, Miao X, Zhang Y, Han S, Wang B, Zhang B, Ye X, Dai Y, Chen C, Rao S, Lin J, Zeng M, Wang H. Time-of-Flight Intracranial MRA at 3 T versus 5 T versus 7 T: Visualization of Distal Small Cerebral Arteries. Radiology 2022;305:E72.
14. Lin L, Liu P, Sun G, Wang J, Liang D, Zheng H, Jin Z, Wang Y. Bi-ventricular assessment with cardiovascular magnetic resonance at 5 Tesla: A pilot study. Front Cardiovasc Med 2022;9:913707.
15. van Osch MJ, Teeuwisse WM, van Walderveen MA, Hendrikse J, Kies DA, van Buchem MA. Can arterial spin labeling detect white matter perfusion signal? Magn Reson Med 2009;62:165-73.
16. Zhao L, Vidorreta M, Soman S, Detre JA, Alsop DC. Improving the robustness of pseudo-continuous arterial spin labeling to off-resonance and pulsatile flow velocity. Magn Reson Med 2017;78:1342-51.
17. Yazici B, Erdoğmuş B, Tugay A. Cerebral blood flow measurements of the extracranial carotid and vertebral arteries with Doppler ultrasonography in healthy adults. Diagn Interv Radiol 2005;11:195-8.
18. Chung S, Kim D, Breton E, Axel L. Rapid B1+ mapping using a preconditioning RF pulse with TurboFLASH readout. Magn Reson Med 2010;64:439-46.
19. Buxton RB, Frank LR, Wong EC, Siewert B, Warach S, Edelman RR. A general kinetic model for quantitative perfusion imaging with arterial spin labeling. Magn Reson Med 1998;40:383-96.
20. Dobre MC, Uğurbil K, Marjanska M. Determination of blood longitudinal relaxation time (T1) at high magnetic field strengths. Magn Reson Imaging 2007;25:733-5.
21. Cheng HL, Wright GA. Rapid high-resolution T(1) mapping by variable flip angles: accurate and precise measurements in the presence of radiofrequency field inhomogeneity. Magn Reson Med 2006;55:566-74.
22. Rolls ET, Huang CC, Lin CP, Feng J, Joliot M. Automated anatomical labelling atlas 3. Neuroimage 2020;206:116189.
23. Lin T, Qu J, Zuo Z, Fan X, You H, Feng F. Test-retest reliability and reproducibility of long-label pseudo-continuous arterial spin labeling. Magn Reson Imaging 2020;73:111-7.
24. Houkin K, Nakayama N, Kuroda S, Nonaka T, Shonai T, Yoshimoto T. Novel magnetic resonance angiography stage grading for moyamoya disease. Cerebrovasc Dis 2005;20:347-54.
25. Xu F, Liu D, Zhu D, Hillis AE, Bakker A, Soldan A, Albert MS, Lin DDM, Qin Q. Test-retest reliability of 3D velocity-selective arterial spin labeling for detecting normal variations of cerebral blood flow. Neuroimage 2023;271:120039.
26. Cohen AD, Agarwal M, Jagra AS, Nencka AS, Meier TB, Lebel RM, McCrea MA, Wang Y. Longitudinal Reproducibility of MR Perfusion Using 3D Pseudocontinuous Arterial Spin Labeling With Hadamard-Encoded Multiple Postlabeling Delays. J Magn Reson Imaging 2020;51:1846-53.
27. Ivanov D, Gardumi A, Haast RAM, Pfeuffer J, Poser BA, Uludağ K. Comparison of 3T and 7T ASL techniques for concurrent functional perfusion and BOLD studies. Neuroimage 2017;156:363-76.
28. Tong Y, Jezzard P, Okell TW, Clarke WT. Improving PCASL at ultra-high field using a VERSE-guided parallel transmission strategy. Magn Reson Med 2020;84:777-86.
29. Fiedler TM, Ladd ME, Bitz AK. SAR Simulations & Safety. Neuroimage 2018;168:33-58.
30. Jahanian H, Noll DC, Hernandez-Garcia L. B0 field inhomogeneity considerations in pseudo-continuous arterial spin labeling (pCASL): effects on tagging efficiency and correction strategy. NMR Biomed 2011;24:1202-9.
31. Luh WM, Talagala SL, Li TQ, Bandettini PA. Pseudo-continuous arterial spin labeling at 7 T for human brain: estimation and correction for off-resonance effects using a Prescan. Magn Reson Med 2013;69:402-10.
32. Wang K, Ma SJ, Shao X, Zhao C, Shou Q, Yan L, Wang DJJ. Optimization of pseudo-continuous arterial spin labeling at 7T with parallel transmission B1 shimming. Magn Reson Med 2022;87:249-62.
33. Chen Y, Wang DJ, Detre JA. Test-retest reliability of

arterial spin labeling with common labeling strategies. J Magn Reson Imaging 2011;33:940-9.
34. Ssali T, Anazodo UC, Bureau Y, MacIntosh BJ, Günther M, St Lawrence K. Mapping Long-Term Functional Changes in Cerebral Blood Flow by Arterial Spin Labeling. PLoS One 2016;11:e0164112.
35. Gevers S, van Osch MJ, Bokkers RP, Kies DA, Teeuwisse WM, Majoie CB, Hendrikse J, Nederveen AJ. Intra- and multicenter reproducibility of pulsed, continuous and pseudo-continuous arterial spin labeling methods for measuring cerebral perfusion. J Cereb Blood Flow Metab 2011;31:1706-15.
36. Mezue M, Segerdahl AR, Okell TW, Chappell MA, Kelly ME, Tracey I. Optimization and reliability of multiple postlabeling delay pseudo-continuous arterial spin labeling during rest and stimulus-induced functional task activation. J Cereb Blood Flow Metab 2014;34:1919-27.
37. Gardener AG, Jezzard P. Investigating white matter perfusion using optimal sampling strategy arterial spin labeling at 7 Tesla. Magn Reson Med 2015;73:2243-8.
38. Ishida S, Kimura H, Isozaki M, Takei N, Fujiwara Y, Kanamoto M, Kosaka N, Matsuda T, Kidoya E. Robust arterial transit time and cerebral blood flow estimation using combined acquisition of Hadamard-encoded multi-delay and long-labeled long-delay pseudo-continuous arterial spin labeling: a simulation and in vivo study. NMR Biomed 2020;33:e4319.
39. Ihara M, Yamamoto Y, Hattori Y, Liu W, Kobayashi H, Ishiyama H, Yoshimoto T, Miyawaki S, Clausen T, Bang OY, Steinberg GK, Tournier-Lasserve E, Koizumi A. Moyamoya disease: diagnosis and interventions. Lancet Neurol 2022;21:747-58.
40. Noguchi T, Kawashima M, Nishihara M, Hirai T, Matsushima T, Irie H. Arterial spin-labeling MR imaging in Moyamoya disease compared with clinical assessments and other MR imaging findings. Eur J Radiol 2013;82:e840-7.
41. Lee S, Yun TJ, Yoo RE, Yoon BW, Kang KM, Choi SH, Kim JH, Kim JE, Sohn CH, Han MH. Monitoring Cerebral Perfusion Changes after Revascularization in Patients with Moyamoya Disease by Using Arterial Spin-labeling MR Imaging. Radiology 2018;288:565-72.

Cite this article as: Fan X, Li Z, Han G, Sun G, Han H, Hong Y, Chen S, You H, Ni J, Li G, Li M, Feng F. Whole-cerebrum three-dimensional pseudo-continuous arterial spin labeling at 5T: reproducibility and preliminary application in moyamoya. Quant Imaging Med Surg 2025;15(5):3824-3838. doi: 10.21037/qims-24-2274

